Feeling Paramagnetic Micro-Particles Trapped Inside Gas Bubbles: A Tele-Manipulation Study

Conference Paper · July 2016

DOI: 10.1109/3M-NANO.2016.7824920

CITATIONS
3

READS
79

4 authors:

Islam S. M. Khalil
University of Twente
178 PUBLICATIONS **1,044** CITATIONS
SEE PROFILE

Youssef Michel
Technische Universität Dortmund
2 PUBLICATIONS **3** CITATIONS
SEE PROFILE

Baiquan Su
Beijing University of Posts and Telecommunications
26 PUBLICATIONS **73** CITATIONS
SEE PROFILE

Sarthak Misra
University of Twente
212 PUBLICATIONS **3,737** CITATIONS
SEE PROFILE

Feeling Paramagnetic Micro-Particles Trapped Inside Gas Bubbles: A Tele-Manipulation Study

Islam S. M. Khalil and Youssef Michel
Department of Mechatronics Engineering
The German University in Cairo
New Cairo, Cairo 11865
Email: islam.shoukry@guc.edu.eg

Baiquan Su
School of Automation, Beijing University
of Posts and Telecommunications
Haidian District, Beijing 100876
Email: subaiquan@bupt.edu.cn

Sarthak Misra
Department of Biomechanical
Engineering, University of Twente
Enschede, 7500 AE
Email: s.misra@utwente.nl

***Abstract*—Surface tension forces, pressure forces, and drag forces arise once a micro-particle comes into contact with a gas bubble or a biological cell in diverse physical and biomedical applications such as targeted therapy, sorting, and characterization of cancer cells. We experimentally demonstrate that these forces can be estimated, scaled-up to the sensory range of a human operator, and sensed during a transparent bilateral tele-manipulation using an electromagnetic system and a haptic device. We find good agreement between the estimated interaction forces and the measured forces using a calibrated microforce sensing probe. The maximum interaction force between a trapped paramagnetic micro-particle and an oxygen bubble is estimated to be 4 μN. The estimated interaction force is scaled-up and used in the design of a tele-manipulation system (haptic device and an electromagnetic system) that enables motion control of the bubble in a two-dimensional space, while sensing the interaction forces with the bubble. We demonstrate experimentally that the operator senses maximum interaction force (surface tension, pressure, and drag forces) with the same order of magnitude as the calculated theoretical forces. The estimation of interaction forces at this scale provides broad possibilities in targeted therapy and characterization of cancer cells.**

I. Introduction

Interaction forces arise during applications such as manipulation of biological cells [1], molecules [2], and high-precision particle separation [3]. Accurate estimation or measurement of these forces to avoid damage is essential for many biological [4], [5] (penetration of cancer cells using nano-motors in targeted drug delivery), physical [6] (study of the particle-to-particle interactions, van der Waals force, and thermophoretic effects), and chemical [7], [8], [9] (catalytic-based micro-motors and nano-particle accumulation) studies. The first controlled manipulation of molecular samples has been achieved by Guthold *et al.* with a nano-manipulator [10]. This nano-manipulator has allowed for the visualization and manipulation of molecular samples using atomic-force microscope (AFM). In biomedical applications, the AFM probes could easily contaminate and damage the walls of the samples during scanning or manipulation. Bukusoglu *et al.* [11] have overcome this problem by achieving haptic manipulation of micro-spheres using optical tweezers and artificial force fields. The micro-manipulation systems become less flexible and difficult to automate due to the scale of the micro- and nano-manipulation, and the predominant adhesive forces (over inertial and gravitational forces). This problem can be overcome by adapting the current tele-manipulation systems [12], [13], [14], [15] to include electromagnetic coils at the slave-side (Fig. 1(a)) to allow for the wireless non-contact micro-manipulation [16], instead of the contact manipulation used by the AFM probes, for instance. We present a theoretical analysis and experimental tele-manipulation of trapped paramagnetic micro-particles inside gas bubbles. First, we analyze the interaction forces of a trapped micro-particle in a gas bubble at the water-gas interface, and we estimate the interaction

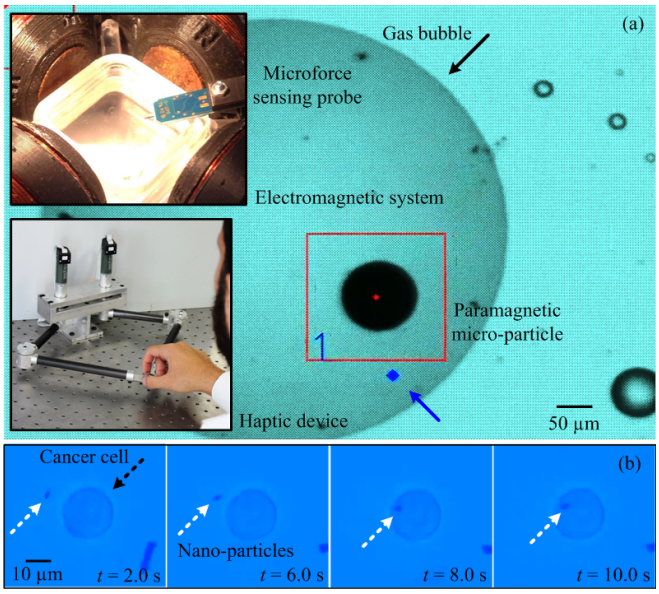

Fig. 1. Electromagnetic-based tele-manipulation of a gas bubble (700 μm in diameter) using a trapped paramagnetic micro-particle (100 μm in diameter). (a) The manipulation is achieved under the influence of the magnetic field gradients exerted on the magnetic dipole of the micro-particle. The controlled gradients are generated using an electromagnetic system (upper-left corner). The interaction forces between the trapped micro-particle and the bubble (black arrow) are measured and scaled-up to the sensory range of the operator (bottom-left inset). The operator moves the micro-particles towards the small blue circle (blue arrow) and feels the scaled drag, pressure, and surface tension forces on the haptic device (bottom-left corner). (b) A potential application of the electromagnetic-based tele-manipulation is targeting and characterization of cancer cells using cluster of nano-particles [5]. The dashed white and black arrows indicate cluster of nano-particles and a cancer cell (U-373 MG human astrocytoma cells).

forces between the micro-particles and the bubble using a calibrated force observer (we expand on the work of [18], [19], [20] which has not verified the accuracy of the estimated forces). This calibration is done using a microforce sensing probe that is incorporated to measure the interaction forces on the micro-particle. The estimation of the interaction forces at this scale and comparison with measured forces is not documented in prior literature. Second, the estimated forces are scaled-up to the sensory range of the operator [21] and used to manipulate gas bubbles in two-dimensional (2D) space under the influence of the controlled magnetic field gradient and using microscopic feedback. The tele-manipulation system consists of a haptic device (pantograph mechanism) and an electromagnetic system with 4 orthogonal electromagnetic coils (Fig. 1(a)). The haptic device allows the operator to provide reference trajectories to the controlled bubble. The electromagnetic configuration surrounds a water reservoir that contains the micro-particles and the gas bubbles (gas bubbles are used instead of biological cell (Fig. 1(b)) to verify the accuracy of the force observer), and their positions are determined using a microscopic system and a high speed camera. The remainder of this paper is organized as follows: Section II provides descriptions pertaining to the interactions between a paramagnetic micro-particle and a gas bubble under the influence of magnetic field and hydrodynamic forces. Section III presents a tele-manipulation control system based on force estimation. Finally, Section IV provides conclusions and directions of future work.

II. Modeling of the Interaction between Paramagnetic Micro-Particle and Gas Bubble

The interactions between the micro-particle and the gas bubble can occur when the micro-particle is outside or trapped inside the bubble, as shown in Fig. 2. The micro-particle is trapped inside a gas bubble manually by ejecting air bubbles gradually using a syringe needle inside a water reservoir that contains the micro-particles. In low-Reynolds-regime fluids, the balance of the force components along the radial direction is given by [22]

$$\mathbf{F_m}(\mathbf{P}) + \mathbf{F_{sp}} + \mathbf{F_p} + \mathbf{F_d}(\dot{\mathbf{P}}) = m\ddot{\mathbf{P}} = 0, \tag{1}$$

where $\mathbf{F_m}(\mathbf{P}) \in \mathbb{R}^{2\times1}$ and $\mathbf{F_{sp}} \in \mathbb{R}^{2\times1}$ are are the magnetic force (at point $\mathbf{P} \in \mathbb{R}^{2\times1}$) and the surface tension force exerted on the micro-particle, respectively. Further, $\mathbf{F_p} \in \mathbb{R}^{2\times1}$ and $\mathbf{F_d} \in \mathbb{R}^{2\times1}$ are the pressure force and the drag force on the micro-particle with mass m, respectively. The inertial term ($m\ddot{\mathbf{P}} \in \mathbb{R}^{2\times1}$) is included in (1) based on the Reynolds number of the micro-particle. For a cluster of less than 4 micro-particles, Reynolds number is calculated to be 0.024 (at average speed of 120 μm/s) and the inertial terms can be neglected in (1). For cluster of 8 micro-particles, Reynolds number is calculated to be 0.19 (at average speed of 494 μm/s). The micro-particles are paramagnetic and consist of iron-oxide in a polylactic acid matrix (PLAParticles-M-redF-plain from Micromod Partikeltechnologie GmbH, Rostock-Warnemuende, Germany). The magnetic force is controlled using the following external magnetic field gradient [23]:

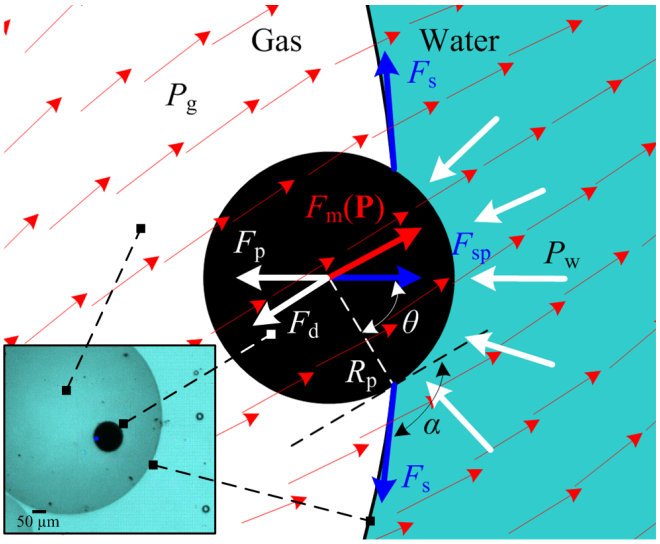

Fig. 2. A schematic representation of the forces exerted on a trapped micro-particles in a gas bubble within a magnetic field. The micro-particles is subjected to magnetic force $\mathbf{F_m}(\mathbf{P})$, surface tension force ($\mathbf{F_{sp}}$), and a pressure force ($\mathbf{F_p}$). The pressure force is generated due to the pressure difference between the gas (P_g) and water (P_w). The red arrows represent the external magnetic fields. The inset shows a microscopic image of a trapped micro-particle inside a gas bubble.

$$\mathbf{F_m}(\mathbf{P}) = \nabla(\mathbf{m}\cdot\mathbf{B}(\mathbf{P})) = \nabla(\mathbf{m}\cdot\tilde{\mathbf{B}}(\mathbf{P})\mathbf{I}). \tag{2}$$

In (2), $\mathbf{m} \in \mathbb{R}^{2\times1}$ and $\mathbf{B}(\mathbf{P}) \in \mathbb{R}^{2\times1}$ are the magnetic dipole moment of the micro-particle and the external magnetic field, respectively. Further, $\tilde{\mathbf{B}}(\mathbf{P}) \in \mathbb{R}^{2\times4}$ and $\mathbf{I} \in \mathbb{R}^{4\times1}$ are the magnetic field-current map [24] and the input current to the electromagnetic coils, respectively. The pressure force exerted on the micro-particles at the water-gas interface is given by [25]

$$\|\mathbf{F_p}\| = \frac{2\pi\gamma}{R_b}(R_p\sin(\theta))^2, \tag{3}$$

where γ is the surface tension. Further, R_p and R_b are the radius of the micro-particle and the radius of the bubble, respectively, and θ is demonstrated in Fig. 2. The pressure force ($\mathbf{F_p}$) is due to the following pressure difference between the gas (P_g) and the water (P_w):

$$P_w - P_g = \frac{2\gamma}{R_b}. \tag{4}$$

The surface tension force ($\mathbf{F_s}$) is given by:

$$\|\mathbf{F_s}\| = 2\pi\gamma R_p \sin\theta. \tag{5}$$

Further, the surface tension force on the micro-particle ($\mathbf{F_{sp}}$) is

$$\mathbf{F_{sp}} = \mathbf{F_s}\sin(|\theta-\gamma|). \tag{6}$$

In (1), the drag force on the trapped micro-particle inside the bubble is calculated using Stokes' law:

$$\mathbf{F_d}(\dot{\mathbf{P}}) = 6\pi\eta R_b\dot{\mathbf{P}}, \tag{7}$$

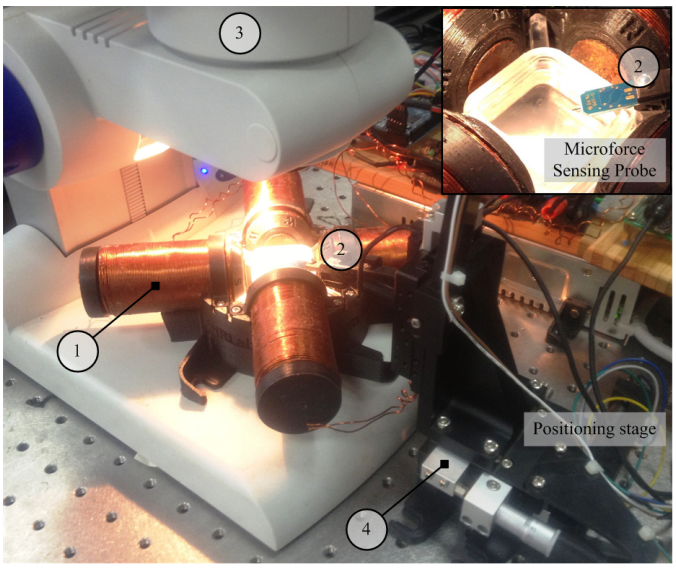

Fig. 3. An electromagnetic system for the bilateral tele-manipulation of paramagnetic micro-particles. The system contains 4 electromagneic coils ① and includes a microforce sensing probe ② to measure the interaction forces with the micro-particle. Motion of the micro-particle is detected using a microscopic system ③, and the microforce sensing probe is positioned using a three-dimensional motion stage ④.

where η is the dynamic viscosity and $\dot{\mathbf{P}}$ is the velocity vector of the bubble (we assume that the trapped micro-particle and the bubble have similar velocity). The input current ($\mathbf{I}$) to the electromagnetic coils and the measured velocity vector of the micro-particle ($\dot{\mathbf{P}}$) are used to estimate the last three forces in (1). The following force observer is used to estimate these forces [18], [26]:

$$\hat{\mathbf{F}}_{\mathbf{par}}(\dot{\mathbf{P}}) = \frac{g}{s+g}\left(\nabla(\mathbf{m}\cdot\tilde{\mathbf{B}}(\mathbf{P})\mathbf{I}) + gm\dot{\mathbf{P}}\right) - gm\dot{\mathbf{P}}), \quad (8)$$

where $\hat{\mathbf{F}}_{\mathbf{par}} \in \mathbb{R}^{2\times 1}$ is the estimated drag, pressure, and surface tension forces on the micro-particle. Further, $g > 0$ is the positive-gain of the force observer. Furthermore, s is the Laplace operator. Experiments are done within a square workspace. The electromagnetic coils provide an average magnetic field ($|\mathbf{B}(\mathbf{P})|$) and field gradient ($\frac{\partial B(\mathbf{P})}{\partial \mathbf{P}}$) within this workspace. The haptic device is a pantograph mechanism that consists of 2 active links of length (l_1) and 2 passive links of length (l_2). Two DC motors (2322 980, Maxon Motor, Sachseln, Switzerland) are used to control the active links. We calculate the net drag, surface tension, and pressure forces on the micro-particle and a gas bubble with average diameters of R_p and R_b, respectively. With the knowledge of the water dynamic viscosity (η) and surface tension (γ) and using the parameters in table 1, the maximum net interaction force (upper-bound) on the micro-particle is calculated to be 8×10^{-6} N, at an average speed of 300 μm.s^{-1}, for the trapped micro-particle in the bubble. In order to verify the accuracy of the force observer (8), we measure the interaction force on a cluster of 3 micro-particles with the tip of the micro-force sensing probe (FT-S100 Microforce Sensing Probe, FemtoTools AG, Buchs, Switzerland). The tip of the micro-force sensing probe is moved gradually to the water-gas interface using a three-dimensional motion stage. The magnetic field gradient (using (2)) provides a pulling force to the micro-particles towards the tip of the probe, as shown in Fig. 4. We observe that the measured force increases gradually as the micro-particles approaches the tip, and a pick force of 0.7 μN is measured, at time, t=6 seconds, upon the contact between the micro-particles and the tip of the sensing probe. Fig. 5 provides a representative comparison between the measured interaction force and the estimated force using (8). This estimation can be controlled by changing the observer gain (g). Increasing this gain provides faster convergence and undesirable measurement noise. Therefore, we set the force observer gain to 10 rad.s^{-1} throughout our experiments, and use (8) in the design of the bilateral tele-manipulation control.

TABLE I

CHARACTERISTICS OF OUR BILATERAL CONTROL SYSTEM. THE SYSTEM CONSISTS OF A HAPTIC DEVICE (MASTER) AS THE PANTOGRAPH MECHANISM AND A MAGNETIC SYSTEM (SLAVE) COMPOSED OF AN ORTHOGNAL ARRAY OF FOUR ELECTROMAGNETS, WITH A WORKSPACE AREA OF 1.3MM×1.3MM.

Parameter	Value	Parameter	Value
m [g]	6.8×10^{-7}	g [rad.s^{-1}]	10
$\lvert\mathbf{B}(\mathbf{P})\rvert$ [mT]	55.9	$\lVert\frac{\partial B(\mathbf{P})}{\partial \mathbf{P}}\rVert$ [T.m^{-1}]	5
R_p [μm]	100	R_b [μm]	700
η [mPa.s]	1.0	γ [N.m^{-1}]	71.97
l_1 [mm]	123	l_2 [mm]	153

III. DESIGN OF BILATERAL CONTROL SYSTEM

As shown in Fig. 3. The red and blue lines represent the measured and estimated interaction forces, respectively (Fig. 4). At time, $t = 1.5$ seconds, the micro-particles touches the tip of the sensor and a peak force of -0.72 μN is measured (compression force). The estimated interaction force (red line) indicates that the observer can be used instead of the force sensor. The fluctuation in the estimated force can be eliminated by decreasing the gain of the force observer (g). However, it is important to consider the trade-off between noise attenuation and convergence speed of the observer [20]. We also estimate the interaction forces between the haptic device and the operator to design the bilateral tele-manipulation system (bottom-left inset in Fig. 1(a)). The interaction force at the haptic device is given by [26]:

$$\hat{\mathbf{F}}_{\mathrm{hap}} = \frac{g}{s+g}\left(\mathbf{K}_\mathrm{t} + g\mathbf{M}_\mathrm{m}\dot{\mathbf{x}}\right) - g\mathbf{M}_\mathrm{m}\dot{\mathbf{x}}, \quad (9)$$

where $\hat{\mathbf{F}}_{\mathrm{hap}} \in \mathbb{R}^{2\times1}$ is the interaction force between the operator and the haptic device. Further, $\mathbf{K}_\mathrm{t} \in \mathbb{R}^{2\times2}$ and $\mathbf{M}_\mathrm{m} \in \mathbb{R}^{2\times2}$ are the matrix of the torque constants of the haptic device and its inertia matrix, respectively. Furthermore, $\dot{\mathbf{x}} \in \mathbb{R}^{2\times1}$ is the velocity vector of the of the interaction point between the operator and the haptic device. The position

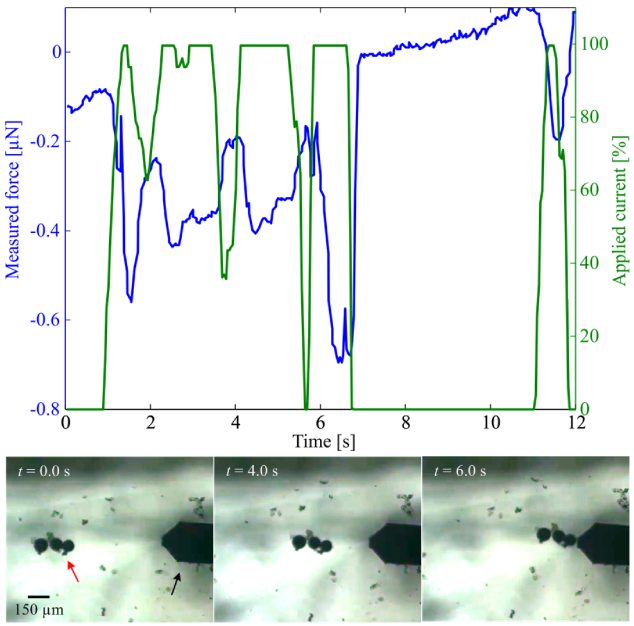

Fig. 4. Measurement of the interaction force between a cluster of 3 paramagnetic microparticles and the tip of a microforce sensing probe (FT-S100 Microforce Sensing Probe, FemtoTools AG, Buchs, Switzerland). The cluster and the microforce sensing probe are indicated using the red and black arrows, respectively. Contact between the cluster and microforce sensing probe occurs after time, t=6 seconds, and a compression force of 0.7 μN is measured.

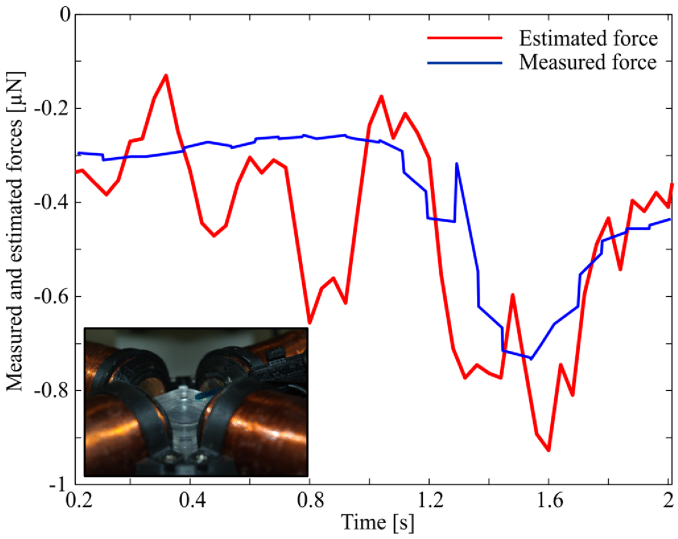

Fig. 5. Comparison between the estimated interaction and measured force. The interaction force is estimated (red line) using (8) and used to design the bilateral tele-manipulation control system. The blue line indicates the measured force during the interaction of a cluster of micro-particles with the tip of a microforce sensing probe (FT-S100 Microforce Sensing Probe, FemtoTools AG, Buchs, Switzerland). A peak-force is measured at time, $t = 1.5$ seconds, during the contact between the micro-particles and the sensor tip. The inset shows the microforce sensing probe and the electromagnetic coils that are used to provide a magnetic force to pull the micro-particles.

($\mathbf{e}_\mathrm{p} \in \mathbb{R}^{2\times1}$) and force ($\mathbf{e}_\mathrm{f} \in \mathbb{R}^{2\times1}$) tracking errors of the tele-manipulation are calculated using

$$\mathbf{e}_\mathrm{p} = \mathbf{x} - \alpha\mathbf{P} \quad \text{and} \quad \mathbf{e}_\mathrm{f} = \hat{\mathbf{F}}_\mathrm{hap} + \beta\hat{\mathbf{F}}_\mathrm{par}, \tag{10}$$

where $\alpha > 0$ and $\beta > 0$ are position and force scaling coefficients, and $\mathbf{x} \in \mathbb{R}^{2\times1}$ is the position of the interaction point between the haptic device and the operator. Using (10), we define a generalized position tracking error ($\sigma \in \mathbb{R}^{2\times1}$) as follows:

$$\sigma = \dot{\mathbf{e}}_\mathrm{p} + c\mathbf{e}_\mathrm{p}. \tag{11}$$

In (11), c is a positive control gain, and finally we devise the following variables to achieve asymptotic convergence:

$$\Gamma_\mathrm{p} = -k_\mathrm{p}\sigma \quad \text{and} \quad \Lambda_\mathrm{f} = -k_\mathrm{f}D_\mathrm{h}^{-1}\mathbf{e}_\mathbf{f}, \tag{12}$$

where $\Gamma_\mathrm{p} \in \mathbb{R}^{2\times1}$ and $\Lambda_\mathrm{f} \in \mathbb{R}^{2\times1}$ are the desired accelerations in the position and force loops, respectively. The tele-manipulation gains ($k_\mathrm{p} > 0$) and ($k_\mathrm{f} > 0$) are positive, and D_h is the damping coefficient of the operator hand. Finally, the control input to the haptic device ($\mathbf{F}$) and the input magnetic force ($\mathbf{F_m}$) are calculated using:

$$\mathbf{F} = \frac{\mathbf{M_m}}{\alpha+\beta}(\alpha\Lambda_\mathrm{f} + \beta\Gamma_\mathrm{p}) \text{ and } \mathbf{F_m} = \frac{\mathbf{1}}{\alpha+\beta}(\Lambda_\mathrm{f} + \Gamma_\mathrm{p}). \tag{13}$$

We substitute (13) in in the equation of motion of the haptic device

$$\mathbf{M}_\mathrm{m}(\mathbf{q})\ddot{\mathbf{x}} + \mathbf{c}_\mathrm{m}(\mathbf{q},\dot{\mathbf{q}}) = \mathbf{F} - \mathbf{f}_\mathrm{o}, \tag{14}$$

where $\mathbf{c}_\mathrm{m}(\mathbf{q},\dot{\mathbf{q}})$ is the Coriolis damping of the haptic device and $\mathbf{f}_\mathrm{o}$ is the interaction force between the haptic device and the operator. This substitution yields the following acceleration:

$$\ddot{\mathbf{x}} = \frac{1}{\alpha+\beta}\left(-\alpha k_\mathrm{f}D_\mathrm{h}^{-1}\mathbf{e}_\mathrm{f} - \beta k_\mathrm{p}\sigma\right). \tag{15}$$

Similarly, subsituting (13) in (1) yields

$$\ddot{\mathbf{P}} = \frac{1}{\alpha+\beta}\left(-\alpha k_\mathrm{f}D_\mathrm{h}^{-1}\mathbf{e}_\mathrm{f} + k_\mathrm{p}\sigma\right). \tag{16}$$

Finally, the position tracking error of the bilateral control system is calculated using (11), (12), (15), and (16), as follows:

$$\ddot{\mathbf{e}}_\mathrm{p} = \ddot{\mathbf{x}} - \alpha\ddot{\mathbf{P}} = -k_\mathrm{p}c\mathbf{e}_\mathrm{p} - k_\mathrm{p}\dot{\mathbf{e}}_\mathrm{p}. \tag{17}$$

Therefore, the error dynamics between the micro-particle and haptic device is governed by

$$\ddot{\mathbf{e}}_\mathrm{p} + k_\mathrm{p}\dot{\mathbf{e}}_\mathrm{p} + k_\mathrm{p}c\mathbf{e}_\mathrm{p} = 0. \tag{18}$$

The control gains k_p and c have to achieve stable roots of the characteristic polynomial of (18). The position of the end-effector of the master-robot is determined via the kinematic equations of the haptic device using its active angles. The position of the micro-particle is determined using a feature tracking algorithm and a microscopic vision system.

Implementation of the control laws (13) is shown in Fig. 6. Force observers (8) and (9) are designed at the haptic device and the electromagnetic configuration, respectively. The operator moves the haptic device and provides reference trajectory (indicated using the small blue circle) in 2D space, as shown in Fig. 6. This reference trajectory is scaled-down (α=2285) to micro-scale to control the motion of the micro-particle based on the motion of the operator. The estimated interaction force

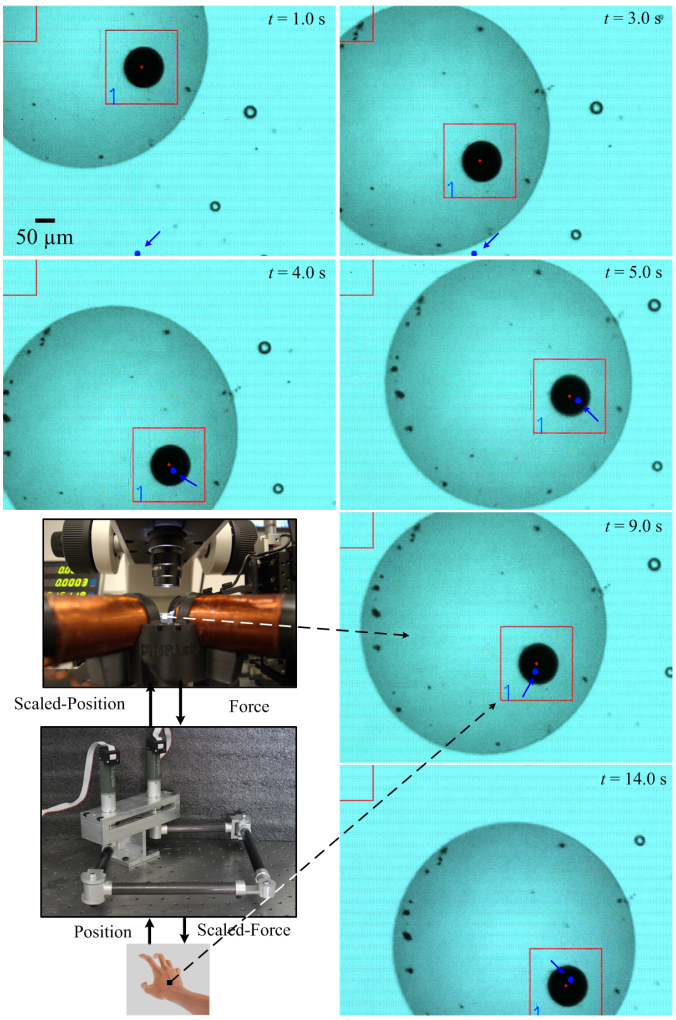

Fig. 6. A representative bilateral tele-manipulation of a gas bubble using a trapped paramagnetic micro-particle. The motion of the micro-particle is controlled under the influence of the magnetic field gradient towards the time-varying reference position (small blue circle) using a haptic device. The interaction forces are sensed on the haptic device after scaling (8) up to the sensory range of the operator.

(using (8)) is scaled-up (by 6 orders on magnitude) to the sensory range of the operator, and sensed on the haptic device, as shown in Fig. 7. In four representative tele-manipulation trials (Fig. 8(a)), the maximum estimated interaction force is calculated to be 4 μN. This estimated interaction force has the same order on magnitude as the calculated forces using (3), (5), and (6). Fig. 8(b) shows the difference between the estimated interaction force between the gas bubble and micro-particle and the scaled force at the haptic device, for each representative trial. We observe that the median force error is approximately 1.86 μN, in the transient-state, whereas the maximum error is calculated to be 8 μN (trial 2). This experiment indicates that the force observer (8) can be used when it is difficult to integrate a microforce sensing probe to the remote micro- or nano-manipulation system.

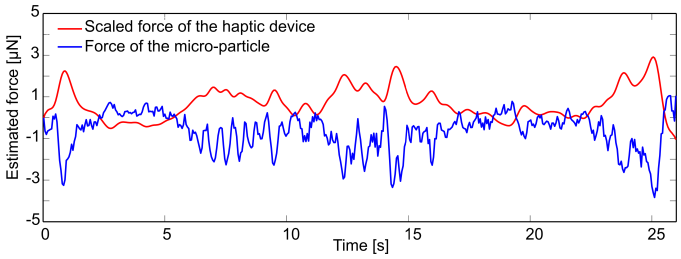

Fig. 7. Estimated forces of the micro-particle and the haptic device (task space forces) during a tele-manipulation trial. The red and blue lines indicate the estimated scaled force of the haptic device and the estimated force of the micro-particles, respectively.

IV. Conclusions and Future Work

In conclusion, we present an experimental study for the tele-manipulation of a gas bubble under the influence of the controlled magnetic fields exerted on a trapped micro-particle. The surface tension forces, pressure forces, and drag forces on the trapped micro-particles are estimated, scaled-up to our sensory range, and sensed by the operator. The estimated force is verified using measurement taken by a calibrated microforce sensing probe, during the interaction of micro-particles with the sensor tip. We also compare the calculated forces and show that they have the same order of magnitude as the scaled sensed force by the operator. The demonstration of the tele-manipulation and scaled sensing of the interaction force with gas bubbles is an important step towards safe manipulation and handling of biological cells in targeted therapy and biomedical applications.

As part of future studies, targeted therapy using tele-manipulation and penetration will be achieved *in vitro*. In addition, the tele-manipulation will be done in three-dimensional space [27]. Furthermore, sorting of cells will be done using our tele-manipulation system with interaction force feedback during the manipulation process to achieve force-controlled manipulation to avoid cell contamination or permanent damage to the cell membrane during contact manipulation.

Acknowledgment

The research leading to these results has received funding from the German University in Cairo and the DAAD-BMBF funding project. The authors would also like to thank Mr. Mahmoud Elfar for collecting the data in Fig. 4.

References

[1] X. L. K. Kim, Y. Zhang, and Y. Sun, "Nanonewton force-controlled manipulation of biological cells using a monolithic MEMS microgripper with two-axis force feedback," in *Journal of Micromechanics and Microengineering*, vol. 18, 055013, April 2008.

[2] S. Fujii, K. Kobayashi, K. Kanaizuka, T. Okamoto, S. Toyabe, E. Muneyuki, and M. Haga, "Manipulation of single DNA using a micronanobubble formed by local laser heating on a Au-coated surface," in *Chemical Letters*, vol. 39, pp. 92–93, December 2010.

[3] F. Petersson, L. Aberg, A. Sward-Nilsson, and T. Laurell, "Free flow acoustophoresis (FFA) - A new microfluidic based mode of particle and cell separation," in *Analytical Chemistry*, vol. 79, pp. 5117-5123, June 2007.

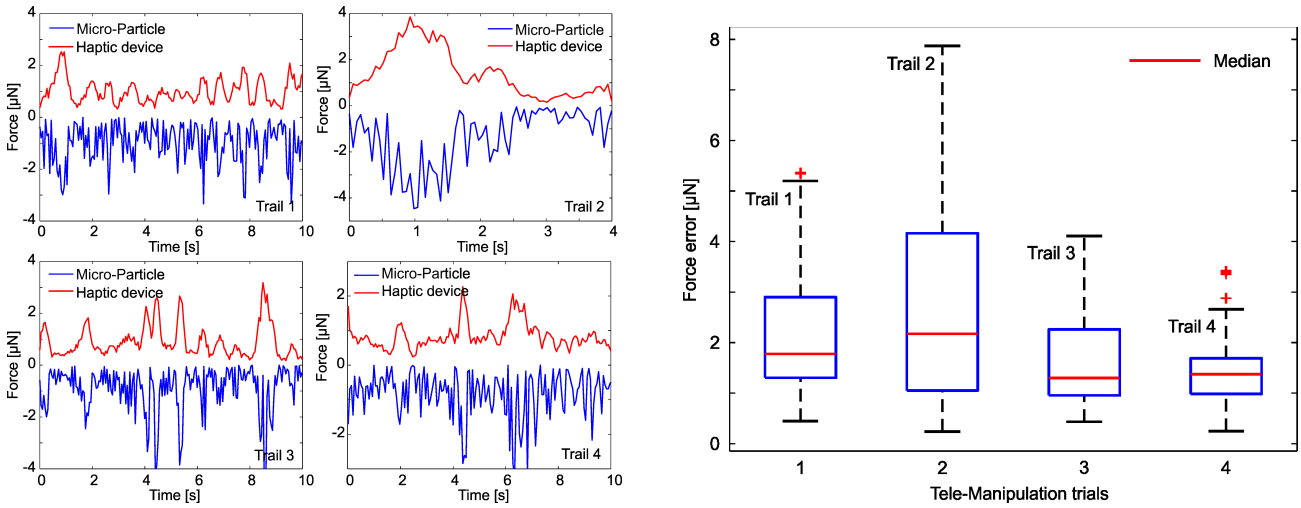

(a) Tele-Manipulation trials

(b) Force error of each trial

Fig. 8. Representative tele-manipulation trials of gas-bubbles using paramagnetic micro-particles. (a) Four tele-manipulation trials of paramagnetic micro-particles, and the interaction forces on the micro-particles (blue line) and haptic device (red line) are measured. These trials are done to allow the operator to sense forces at the micro-scale. (b) The median force error is approximately 1.86 μN.

[4] W. Wang, S. Li, L. Mair, S. Ahmed, T. J. Huang, and T. E. Mallouk, "Acoustic propulsion of nanorod motors inside living cells," in *Angewandte Chemie International Edition*, vol. 53, pp. 3201-3204, February 2014.

[5] I. S. M. Khalil, I. E. O. Gomaa, R. M. Abdel-Kader, and S. Misra, "Magnetic-Based contact and non-contact manipulation of cell mockups and MCF-7 human breast cancer cells," *Smart Drug Delivery System*, Intech, ch. 9, pp. 219-235, February 2016.

[6] L. Zhang, J. J. Abbott, L. Dong, B. E. Kratochvil, D. Bell, and B. J. Nelson, "Artificial bacterial flagella: fabrication and magnetic control," in *Applied Physics Letters*, vol. 94, 064107, February 2009.

[7] S. Sanchez, A. A. Solovev, S. Schulze, and O. G. Schmidt, "Controlled manipulation of multiple cells using catalytic microbots," in *Chemical Communication*, vol. 47, pp. 698-700, November 2010.

[8] I. S. M. Khalil, V. Magdanz, S. Sanchez, O. G. Schmidt, and S. Misra, "Three-dimensional closed-loop control of self-propelled microjets," in *Applied Physics Letters*, vol. 103, 172404, October 2013.

[9] A. A. Solovev, S. Sanchez, M. Pumera, Y. F. Mei, and O. G. Schmidt, "Magnetic control of tubular catalytic microbots for the transport, assembly," in *Advanced Functional Materials*, vol. 20, pp. 2430-2435, June 2010.

[10] M. Guthold, M. Falvo, W. Matthews, S. Paulson, S. Washburn, D. Erie, R. Superfine, F. P. Brooks, and R. M. Taylor, "Controlled manipulation of molecular samples with the nanoManipulator," in *IEEE/ASME Transactions on Mechatronics*, vol. 5, pp. 189-198, June 2000.

[11] I. Bukusoglu, C. Basdogan, A. Kiraz, and A. Kurt, "Haptic manipulation of microspheres using optical tweezers under the guidance of artificial force fields," in *Presence: Teleoperators Virtual Environments,* vol. 17, pp. 344-364, August 2008.

[12] A. Bolopion, H. Xie, D. S. Haliyo, and S. Regnier, "Haptic teleoperation for 3-D microassembly of spherical objects," in *IEEE/ASME Transactions on Mechatronics,* vol. 17, pp. 116-127, December 2010.

[13] C. D. Onal and M. Sitti, "Task-based and stable telenanomanipulation in a nanoscale virtual environment," in *The International Journal of Robotic Research,* vol. 28, pp. 240-247, July 2006.

[14] K. Takeo and K. Kosuge, "Implementation of the micro-macro teleoperation system without using slave-side force sensors," in *Proceedings of the IEEE International Conference on Robotics and Automation (ICRA)*, pp. 1600–1605, Albuquerque, USA, April 1997.

[15] A. Ferreira and C. Mavroidis,"Virtual reality and haptics for nanorobotics," in *IEEE Robotics & Automation Magazine,* vol. 13, pp. 78-92, August 2006.

[16] A. G. El-Gazzar, L. E. Al-Khouly, A. Klingner, S. Misra and I. S. M. Khalil, "Non-Contact manipulation of microbeads via pushing and pulling using magnetically controlled clusters of paramagnetic microparticles," in *Proceedings of the IEEE/RSJ International Conference of Robotics and Systems (IROS)*, pp. 778–783, Hamburg, Germany, October 2015.

[17] K. Youakim, M. Ehab O. Hatem, S. Misra, and I. S. M. Khalil, "Paramagnetic microparticles sliding on a surface: characterization and closed-loop motion control," *Proceedings of the IEEE International Conference on Robotics and Automation (ICRA)*, pp. 4068-4073, Seattle, USA, May 2015.

[18] I. S. M. Khalil, L. Abelmann, and S. Misra, "Magnetic-Based motion control of paramagnetic microparticles with disturbance compensation," in *IEEE Transactions on Magnetics*, vol. 50, 5400110, May 2014.

[19] I. S. M. Khalil, A. Sabanovic, and S. Misra, "An energy-based state observer for dynamical subsystems with inaccessible state variables", in *Proceedings of the IEEE International Conference on Intelligent Robots and Systems (IROS)*, Vilamoura, Portugal, pp. 3734-3740, October 2012.

[20] I. S. M. Khalil, R. M. P. Metz, L. Abelmann, and S. Misra, "Interaction force estimation during manipulation of microparticles," *Proceedings of the IEEE/RSJ International Conference of Robotics and Systems (IROS)*, pp. 950–956, Vilamoura, Algarve, Portugal, October 2012.

[21] L. Skedung, M. Arvidsson, J. Y. Chung, C. M. Stafford, B. Berglund, and M. W. Rutland, "Feeling small: exploring the tactile perception limits," in *IEEE/ASME Scientific Reports,* vol. 3, pp. 2617, September 2013.

[22] A. W. Adamson and G. P. Alice, "Physical chemistry of surfaces," 6th edition, Wiley Interscience.

[23] M. E. Alshafeei, A. Hosney, A. Klingner, S. Misra, and I. S. M. Khalil, "Magnetic-Based motion control of a helical robot using two synchronized rotating dipole fields," in *Proceedings of the IEEE RAS/EMBS International Conference on Biomedical Robotics and Biomechatronics (BioRob)*, pp. 151-156, São Paulo, Brazil, August 2014.

[24] M. P. Kummer, J. J. Abbott, B. E. Kartochvil, R. Borer, A. Sengul, and B. J. Nelson, "OctoMag: An electromagnetic system for 5-DOF wireless micromanipulation," in *IEEE Transactions on Robotics,* vol. 26, pp. 1006-1017, December 2010.

[25] C. Zhao, Y. Xie, Z. Maoa, Y. Zhaoa, J. R. S. Yanga, F. Guoa, J. D. Maic, and T. J. Huang, "Theory and experiment on particle trapping and manipulation via optothermally generated bubbles," in *Lab on a Chip*, vol. 14, pp. 384-391, January 2014.

[26] T. Murakami and K. Ohnishi, "Observer-based motion control application to robust control and parameter identification," in *Asia-Pacific Workshop on Advances in Motion Control (AMC),* pp. 1-6, July 1993.

[27] I. S. M. Khalil, R. M. P. Metz, B. A. Reefman, and S. Misra, "Magnetic-Based minimum input motion control of paramagnetic microparticles in three-dimensional space," *Proceedings of the IEEE/RSJ International Conference of Robotics and Systems (IROS)*, pp. 2053-2058, Tokyo, Japan, November 2013.